Modeling, Full Identification and Control of the Mitsubishi PA-10 Robot Arm

Nikolaos A. Bompos   Panagiotis K. Artemiadis*   Apollon S. Oikonomopoulos   Kostas J. Kyriakopoulos

Control Systems Lab, School of Mechanical Eng.
National Technical University of Athens,
9 Heroon Polytechniou Str, Athens, 157 80, Greece
{mc00123,partem,apollon,kkyria}@mail.ntua.gr
*corresponding author

Abstract— **This paper presents the modeling, identification and control of the 7 degrees of freedom (DoFs) Mitsubishi PA-10 robot arm. The backdrivability, high accuracy positioning capabilities and zero backlash afforded by its harmonic drive transmission, make the PA-10 ideal for precise manipulation tasks. However, the lack of any technical knowledge on the dynamic parameters of its links and the non linear characteristics of friction at its joints, make the development of an accurate dynamic model of the robot extremely challenging. The innovation of this research focuses on the development of the full dynamic model of the PA-10 robot arm, the development of a new non linear model for the friction at its joints, the estimation of the stiffness characteristics of its joints and finally the full identification of the dynamic parameters of the robot arm. The accuracy of the full dynamic model identified is proved by an end-effector trajectory tracking task using a model-based inverse dynamic controller.**

Index Terms— **Robot parameter identification, robot friction, dynamics**

I. INTRODUCTION

The accurate modeling of the dynamics of robot manipulators has received increased attention, as dexterous manipulation tasks and interaction with the environment demand the knowledge of the full dynamic model of the robot. Dynamic models of robot arms used in model-based control schemes are designed in terms of various inertial and friction parameters that must be either measured directly or determined experimentally. However, direct measurements of such characteristics are rather impractical or even impossible in many cases. Inertial parameters of robot links can not be measured without dismantling the robot arm, while highly non-linear inherent phenomena at robot joints can not be directly quantified. Therefore, models describing nonlinear effects such as friction, should be addressed in conjunction with methods of determining parameters of the dynamic model of the arm based on experiments, in order to fully identify the dynamic model of the robot arm.

The Mitsubishi PA-10 is a 7 degrees of freedom (DoFs) robot arm, widely used due to the backdrivability, accurate positioning and zero backlash afforded by its harmonic drive transmission. Its relatively small volume along with the dexterity provided by the redundancy in DoFs, entail its usage in demanding tasks such as surgical tool placement or teleoperated soft tissue manipulation. However, the inherent compliance and non-linear friction in its harmonic drive system make the development of an accurate dynamic model of the robot an extremely challenging issue.

Modeling of the PA-10 transmission system has been addressed in low velocity, low impedance implementation in [1]. In that approach, the dynamic model of the harmonic drive transmission was developed, for low velocity applications. The friction effects were modeled using a Stribeck model, while the stiffness of the harmonic drives was modeled using a combination of linear functions for each joint. However, the inertial effects of the robot arm were neglected due to low velocity implementation, while the redundant DoF (joint 3) was neglected during the end-effector tracking experiments. Focusing on the area of modeling of harmonic drive systems, an overview of modeling and parameter identification of such systems in [2] is worth noticing. Kircanski [3] provided a detailed analysis of the nonlinear behavior of harmonic gears due to compliance, friction and hysteresis, while Taghirad [4] presented a control scheme for harmonic drive systems based on experimentally identified models for the inherent dynamics of those. However, most of these works are tested in custom-designed experimental platforms, that allow direct measurement of system parameters such as compliance and kinematic transmission error. In commercial robotic manipulators though, like the PA-10, those measurements are not available.

Friction modeling in robotic manipulators has been widely analyzed in [5]. A presentation of methodologies developed for experimentally determining accurate models of non-linear friction is addressed in [6], while an analysis of various friction models has been implemented in [7]. Dynamic parameter identification of robotic manipulators has been widely analyzed in [8], while a method for determining parameters of a dynamic robot model based on experiments is presented in [9].

In this paper, the modeling, full identification and control of the Mitsubishi PA-10 robot arm are implemented. A new non-linear model for the friction phenomenon at the PA-10 harmonic drive system is introduced and experimentally verified, while a model for the effect of stiffness of the robot joints is developed. Then, after transforming the dynamic model of the robot arm to an identifiable form, the full set of dynamic parameters is identified through experiments. The accuracy of the identified model is verified through end-effector trajectory tracking experiments, using a model-based inverse dynamic
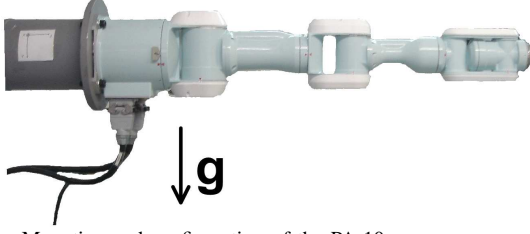
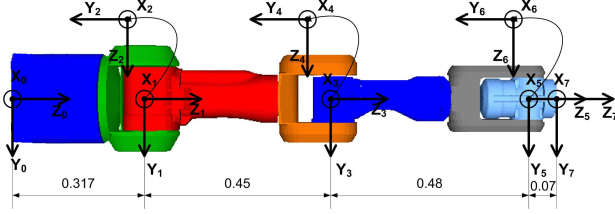Fig. 1. Mounting and configuration of the PA-10.

Fig. 2. Links and frames assignment of the PA-10. Dimensions are given in m.

controller. Consequently, the novelty of this paper focuses on the methodology consisting of the full identification of inertial, friction and stiffness characteristics of the PA-10 robot arm, at a variety of velocity and load conditions.

The rest of the paper is organized as follows: Section II gives a description of the modeling methodology proposed, with the appropriate segregation of the distributed sub-problems of dynamic modeling and nonlinear friction modeling and stiffness identification. Section III illustrates the experimental results of the full model identification of the robot arm through the implementation of a model-based inverse dynamic controller, while section IV concludes the paper.

II. MODELING

A. Dynamic Model

The Mitsubishi PA-10 robot arm has 7 rotational DoFs, arranged in an anthropomorphic way: 2 DoFs at the shoulder, 2 DoFs at the elbow, and 3 DoFs at the wrist. The robot servo controller communicates with a personal computer (PC) via the ARCNET protocol. The robot arm can be controlled either at "velocity mode" where the desired joint velocity is commanded from the PC, or at "torque mode" where the desired joint torque is commanded. For the identification of the full robot arm model, the "velocity mode" is used.

The PA-10 has been mounted in an horizontal way as shown in Fig. 1. The links of the robot arm along with their frames are shown in Fig. 2. The frames are assigned using the modified Denavit-Hartenberg (D-H) notation [10]. The modified D-H parameters are listed in Table I, while the relation between frame $i-1$ and i is given by

$$
{}^{i-1}_{i}T = \begin{bmatrix} c\theta_i & -s\theta_i & 0 & a_{i-1} \\ s\theta_i c\alpha_{i-1} & c\theta_i c\alpha_{i-1} & -s\alpha_{i-1} & -s\alpha_{i-1}d_i \\ s\theta_i s\alpha_{i-1} & c\theta_i s\alpha_{i-1} & c\alpha_{i-1} & c\alpha_{i-1}d_i \\ 0 & 0 & 0 & 1 \end{bmatrix}
$$
(1)

where c, s correspond to cos and sin respectively. In Fig. 2, each link is denoted with different color, and the numbering

i	α_{i-1}	a_{i-1}	d_i	θ_i
1	0	0	0.317	q_1
2	$-90°$	0	0	q_2
3	$90°$	0	0.45	q_3
4	$-90°$	0	0	q_4
5	$90°$	0	0.48	q_5
6	$-90°$	0	0	q_6
7	$90°$	0	0.07	q_7

starts from 0. The dynamic model of the robot arm is constructed using the Lagrange equations expressed by

$$
\frac{d}{dt}\frac{\partial L}{\partial \dot{q}_i} - \frac{\partial L}{\partial q_i} = \tau_i \quad , i = 1, \ldots, 7
$$
(2)

where q_i the joint angles, $\dot{q}_i$ the joint velocities, τ_i the joint torques and L is defined by

$$
L = T - U
$$
(3)

where T and U are the total kinetic energy and potential energy of the system respectively, defined by

$$
T = \sum_{i=0}^{6} T_i \quad U = \sum_{i=0}^{6} U_i
$$
(4)

where T_i, U_i the kinetic and potential energy of link i respectively. If the augmented link i is defined as the combination of link i and motor $i+1$, then the kinetic energy of the augmented link i is given by

$$
T_i = \frac{1}{2}m_i\dot{\mathbf{p}}_i^{iT}\dot{\mathbf{p}}_i^{i} + \dot{\mathbf{p}}_i^{iT}\mathbf{S}\left(\omega_i^i\right)m_i\mathbf{r}_{i,C_i}^{i} + \frac{1}{2}\omega_i^{iT}\hat{\mathbf{I}}_i^i\omega_i^i \\ + k_{r,i+1}\dot{q}_{i+1}I_{m_{i+1}}\mathbf{z}_{m_{i+1}}^{iT}\omega_i^i + \frac{1}{2}k_{r,i+1}^2\dot{q}_{i+1}^2 I_{m_{i+1}}
$$
(5)

where

m_i: the overall mass of the augmented link i,

$\dot{\mathbf{p}}_i^i$: the linear velocity of the link i referred to frame i

ω_i^i : the angular velocity of link i expressed with reference to frame i

$\mathbf{r}_{i,C_i}^i$: the vector with start the reference frame i and end the center of mass of the augmented link i, referred to frame i,

$k_{r,i+1}$: the gear reduction ratio of motor $i+1$,

$I_{m_{i+1}}$: the inertia tensor of the rotor $i+1$ relative to its center of mass,

$\mathbf{z}_{m_{i+1}}^i$: the unit vector along the rotor axis $i+1$ referred to frame i,

$\mathbf{S}\left(\cdot\right)$: a matrix operator defined for a vector $\mathbf{r} = \begin{bmatrix} r_x & r_y & r_z \end{bmatrix}^T$ by

$$
\mathbf{S}\left(\mathbf{r}\right) = \begin{bmatrix} 0 & -r_z & r_y \\ r_z & 0 & -r_x \\ -r_y & r_x & 0 \end{bmatrix}
$$
(6)

$\hat{\mathbf{I}}_i^i$: the inertia tensor of the augmented link i with respect to the origin of frame i, given by

$$
\hat{\mathbf{I}}_i^i = \begin{bmatrix} \hat{I}_{ixx} & -\hat{I}_{ixy} & -\hat{I}_{ixz} \\ -\hat{I}_{ixy} & \hat{I}_{iyy} & -\hat{I}_{iyz} \\ -\hat{I}_{ixz} & -\hat{I}_{iyz} & \hat{I}_{izz} \end{bmatrix}
$$
(7)

The potential energy of the augmented link i is given by

$$U_i = -\mathbf{g}_0^{iT}\left(m_i\mathbf{p}_i^i + m_i\mathbf{r}_{i,C_i}^i\right) \tag{8}$$

where $\mathbf{p}_i^i$ the position vector of link i referred to frame i and $\mathbf{g}_0^i$ the gravity acceleration vector referred to frame i [11]. If $\mathbf{r}_{i,C_i}^i$ is defined by

$$r_{i,C_i}^i = \begin{bmatrix} \ell_{C_ix} & \ell_{C_iy} & \ell_{C_iz} \end{bmatrix}^T \tag{9}$$

then the Lagrangian of the system can be expressed by

$$L = \sum_{i=1}^{7}\left(\beta_{T_i}^T - \beta_{U_i}^T\right)\pi_i \tag{10}$$

where π_i is the 11×1 vector of dynamic parameters defined by

$$\pi_i = \begin{bmatrix} m_i & m_i\ell_{C_ix} & m_i\ell_{C_iy} & m_i\ell_{C_iz} \\ \hat{I}_{ixx} & \hat{I}_{ixy} & \hat{I}_{ixz} & \hat{I}_{iyy} & \hat{I}_{iyz} & \hat{I}_{izz} & I_{m_{i+1}} \end{bmatrix}^T \tag{11}$$

and β_{T_i}, β_{U_i} 11×1 vectors that are dependent on joint positions q_i and joint velocities $\dot{q}_i$. The derivation required by the Lagrange's equation (2) does not alter the property of linearity in the parameters. Therefore, for the total links of the robot arm, it is

$$\tau = \mathbf{Y}\left(\mathbf{q},\dot{\mathbf{q}},\ddot{\mathbf{q}}\right)\pi \tag{12}$$

where τ a 7×1 vector of joint torques, π a p×1 vector of constant parameters and $\mathbf{Y}$ a 7×p matrix which is a function of joint positions, velocities and accelerations. Considering the PA-10 robot arm and (11), π is initially a 77×1 vector, omitting friction parameters. For the purpose of the identification of the parameter vector π, the base parameters should be determined, since they constitute the only identifiable parameters. These base parameters can be deduced from the standard parameters by eliminating those that have no effect on the dynamic model and by grouping some others.

The center of mass for each augmented link i is located on the axis passing through the center of the frames i and $i+1$ as reported by mass distribution drawings provided by Mitsubishi Heavy Industries [12]. Due to this fact, the following simplification can be made:

$$\ell_{C_1x} = \ell_{C_1y} = \ell_{C_2x} = \ell_{C_2z} = \ell_{C_3x} = \ell_{C_3y} = \\ \ell_{C_4x} = \ell_{C_4z} = \ell_{C_5x} = \ell_{C_5y} = \ell_{C_6x} = \ell_{C_6z} = 0 \tag{13}$$

Moreover, due to specific symmetries of the links, the following simplifications can be made:

$$\hat{I}_{1xz} = \hat{I}_{1xy} = \hat{I}_{1yz} = \hat{I}_{2xy} = \hat{I}_{2xz} = \hat{I}_{3xz} = \\ \hat{I}_{3xy} = \hat{I}_{3yz} = \hat{I}_{4xy} = \hat{I}_{4xz} = \hat{I}_{5xz} = \hat{I}_{5xy} = \\ \hat{I}_{5yz} = \hat{I}_{6xz} = \hat{I}_{6xy} = \hat{I}_{6yz} = 0 \tag{14}$$

For the determination of the base parameters, a straightforward closed-loop form method is used [13]. If j a revolute joint, between links j and $j-1$, then the resulting grouped

parameters are given by

$$I_{jxxR} = I_{jxx} - I_{jyy}$$
$$I_{(j-1)xxR} = I_{(j-1)xx} + I_{jyy} + 2d_jM_{jz} + d_j^2M_j$$
$$I_{(j-1)xyR} = I_{(j-1)xy} + a_{j-1}S\alpha_{j-1}M_{jz} + a_{j-1}d_jS\alpha_{j-1}M_j$$
$$I_{(j-1)xzR} = I_{(j-1)xz} - a_{j-1}C\alpha_{j-1}M_{jz} - a_{j-1}d_jC\alpha_{j-1}M_j$$
$$I_{(j-1)yyR} = I_{(j-1)yy} + CC\alpha_{j-1}I_{jyy} + 2d_jCC\alpha_{j-1}M_{jz} \\ + \left(a_{j-1}^2 + d_j^2CC\alpha_{j-1}\right)M_j$$
$$I_{(j-1)yzR} = I_{(j-1)yz} + CS\alpha_{j-1}I_{jyy} + 2d_jCS\alpha_{j-1}M_{jz} \\ + d_j^2CS\alpha_{j-1}M_j$$
$$I_{(j-1)zzR} = I_{(j-1)zz} + SS\alpha_{j-1}I_{jyy} + 2d_jSS\alpha_{j-1}M_{jz} \\ + \left(a_{j-1}^2 + d_j^2SS\alpha_{j-1}\right)M_j$$
$$M_{(j-1)xR} = M_{(j-1)x} + a_{j-1}M_j$$
$$M_{(j-1)yR} = M_{(j-1)y} - S\alpha_{j-1}M_{jz} - d_jS\alpha_{j-1}M_j$$
$$M_{(j-1)zR} = M_{(j-1)z} + C\alpha_{j-1}N_{jz} + d_jC\alpha_{j-1}M_j$$
$$M_{(j-1)R} = M_{(j-1)} + M_j \tag{15}$$

where: $SS\left(\cdot\right) = \sin\left(\cdot\right)\sin\left(\cdot\right)$, $CC\left(\cdot\right) = \cos\left(\cdot\right)\cos\left(\cdot\right)$, $CS\left(\cdot\right) = \cos\left(\cdot\right)\sin\left(\cdot\right)$,
I_{jxxR}: the grouped inertial parameter corresponding to link j with respect to the x axis,
I_{jxx}: the moment of inertia of link j with respect to the x axis,
M_{jz}: the first moment of inertia of link j with respect to the z axis, corresponding to $m_i\ell_{C_iz}$ in (11)
M_j: the mass of the link j, , corresponding to m_i in (11)
$M_{(j-1)xR}$: the grouped parameter corresponding to the first moment of inertia of link $j-1$ with respect to the x axis
$M_{(j-1)R}$: the grouped parameter corresponding to the mass of the link $j-1$.
All the other symbol definitions can be resulted from the above. Considering augmented links used in (5) and using (15), the final base parameter vector of the PA-10 robot arm is given by:

$$\pi = \begin{bmatrix} \hat{I}_{1zzR} & M_{2yR} & \hat{I}_{2xxR} & \hat{I}_{2yzR} & \hat{I}_{2zzR} & I_{m_3} & \hat{I}_{3xxR} \\ \hat{I}_{3zzR} & I_{m_4} & M_{4yR} & \hat{I}_{4xxR} & \hat{I}_{4yzR} & \hat{I}_{4zzR} & I_{m_5} \\ \hat{I}_{5xxR} & \hat{I}_{5zzR} & I_{m_6} & M_{6yR} & \hat{I}_{6xxR} & \hat{I}_{6zzR} & I_{m_7} \end{bmatrix}^T \tag{16}$$

where the relation between the 21 base parameters with the PA-10 augmented link parameters of (11) is defined in Appendix. The matrix multiplication of the 21×1 base parameter vector with the corresponding 7×21 $\mathbf{Y}$ matrix was tested to result to the same expression, as this resulted from (12) in symbolic form, using the Mathematica® software package. Moreover, using the grouped parameter Y matrix, the dynamic model equation was written in the following form:

$$B\left(q\right)\ddot{q} + C\left(q,\dot{q}\right)\dot{q} + G\left(q\right) + F = \tau \tag{17}$$

where $B\left(q\right)$ the 7×7 inertia matrix, $C\left(q,\dot{q}\right)$ the 7×7 Coriolis-Centrifugal matrix, $G\left(q\right)$ the gravity vector and F the vector of friction analyzed in following section.

B. Friction Model

For the identification of the friction forces, a large number of constant velocity experiments were conducted for each of the seven joints, controlling the arm in "velocity mode", in such a configuration that gravity did not affect joint motion.

TABLE II
FRICTION COEFFICIENTS

	Positive Velocity					
Joint	f_1	f_2	f_3	f_4	f_5	f_6
1	0.4362	0.6632	0.4469	0.0622	0.5612	16.9787
2	0.2896	0.7659	0.5445	0.0202	0.4498	48.4405
3	0.1434	0.3302	0.2499	0.0537	0.2991	16.6124
4	0.0640	0.0922	-0.0954	0.1767	-0.1283	39.4975
5	0.0231	0.1198	0.1045	0.1060	0.1005	11.4160
6	0.0551	0.0829	0.0373	0.0220	0.0	0.0
7	0.0304	0.1102	0.0895	0.1605	0.1073	8.3338
	Negative Velocity					
1	0.3952	0.8550	0.6203	0.0583	0.7244	19.1778
2	0.1960	0.7482	0.4624	0.0215	0.3744	38.7804
3	0.1391	0.3576	0.2451	0.1073	0.3389	10.0974
4	0.0690	0.1122	-0.0626	0.4307	-0.0919	-101.92
5	0.0337	0.0796	0.0378	1.2697	0.1047	1.0697
6	0.0390	0.0846	0.0286	0.0411	0.0	0.0
7	0.0273	0.1070	0.0841	0.1683	0.1008	8.0266

It was noticed that the friction torque at the most joints had the above characteristics:

1) Static friction was noticed less than kinetic friction and the rise from static does not occur instantly.
2) Kinetic friction was noticed more than viscous friction within the low velocity region, while the drop from kinetic to low-velocity viscous does not occur instantly.

It must be noted that static friction was defined as the torque needed to initiate a motion with constant velocity of $0.001rad/sec$. From the above characteristics of friction it can be concluded that a Stribeck model is inadequate for the case of PA-10 [5]. Therefore, a new term has been added to the Stribeck model, concluding to a new model for friction given by:

$$F = f_1\dot{q} + f_2 sign\left(\dot{q}\right) - f_3 sign\left(\dot{q}\right)e^{-\frac{|\dot{q}|}{f_4}} - f_5 sign\left(\dot{q}\right)e^{-\frac{1}{f_6|\dot{q}|}} \tag{18}$$

where $f_i, i = 1,...,6$ the model coefficients. It must be noted that the new term $f_5 sign\left(\dot{q}\right)e^{-\frac{1}{f_6|\dot{q}|}}$ was added to account for the second specific characteristic of friction discussed above, i.e. the drop in friction force from kinetic to low-velocity viscous friction. Experiments of constant velocity conducted for velocities ranging from $0.001rad/sec$ to 60% of maximum value for each joint. Experimental results along with the fitted model of form defined in (18) are shown in Fig. 3-5. Torque values correspond to motor axis, before transmission. The friction model coefficients, computed by applying the nonlinear least squared method, are listed in Table II. Friction was noticed to be non-symmetric at positive and negative velocities. It must be noted that each joint was forced to one minute of moderate velocity activity spanning the workspace, before the identification of the friction model, as suggested in [5].

C. Stiffness Model

Harmonic drives exhibit significant compliance when externally loaded [1]. Experimental tests in [2] indicate that stiffness in harmonic drives increases with increasing load. Direct measurement of stiffness entails the measurement of position in both motor side and joint side. However, this is
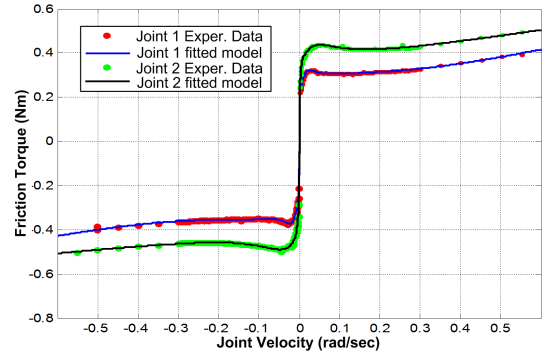

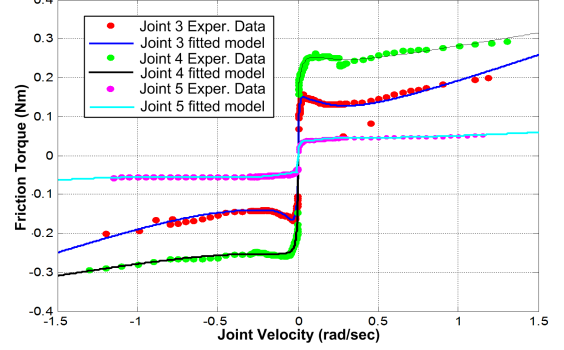Fig. 3. Joints 1, 2: Friction experimental data and fitted curve.

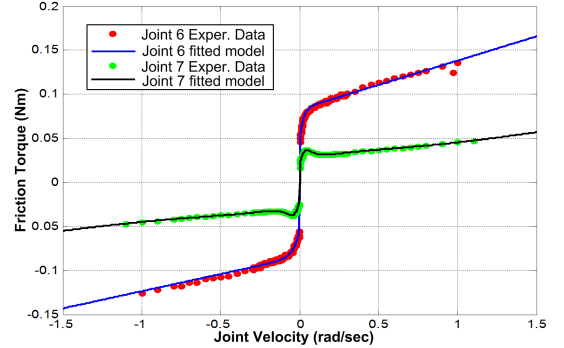Fig. 4. Joints 3, 4, 5: Friction experimental data and fitted curve.

Fig. 5. Joint 6, 7: Friction experimental data and fitted curve.

impossible in commercial robots. Therefore the determination of the torque used to deform the compliant elements of the joint transmissions can only be accomplished through the torque measurements during loaded conditions. The experiments conducted on the PA-10 robot arm using as load for each joint the weight of its following links, revealed that joint transmission compliance has a significant effect on the robot arm dynamics. Each joint was commanded to move at constant velocity, in such configuration that gravity due to its following links affected its motion. The torque due to joint transmission stiffness was computed by subtracting friction and gravitational terms from the total torque measured. The gravitational term of torque for each joint is computed using the G vector in (17) and the data provided by Mitsubishi [12]. Experimental results revealed that stiffness effect is present at joints 1-4, while joint 5-7 are not considerably affected. In Fig. 6, the stiffness experimental data and fitted linear models are depicted, while the torque values given correspond to the
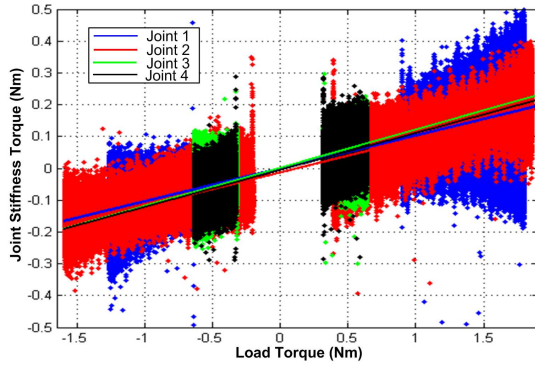
Fig. 6. Stiffness experimental data and fitted models for Joints 1-4. Experimental values are depicted as dots while fitted model as lines of the same color.

Fig. 7. End-effector trajectory tracking performance.

motor axis. The fitted linear models are given by:

$$
\begin{aligned}
S_1 &= 0.1036\tau_{L_1} - 2.817 \cdot 10^{-5} \\
S_2 &= 0.1054\tau_{L_2} - 0.01256 \\
S_3 &= 0.1199\tau_{L_3} + 0.00192 \\
S_4 &= 0.1161\tau_{L_4} - 0.00488
\end{aligned}
\tag{19}
$$

where S_i the stiffness torque, τ_{L_i} the load torque, while the coefficients are calculated using least squares method. for each joint $i = 1, .., 4$.

III. EXPERIMENTAL RESULTS

A. System Components

The experimental setup consisted of the PA-10, its servo-controller and a PC running GNU/Linux connected to it via the ARCNET interface. The control of the robotic arm was realized by means of a custom multi-threaded C library, based on the Linux kernel's ARCNET driver and providing an Application Programming Interface (API) featuring almost all of the capabilities of the PA-10. The library acquires its timing through a High Resolution POSIX Timer, with a resolution of 10 μsec, which, combined with the preemption features of the modern Linux kernels, offers a 99.9% steady communication cycle of 2.5 ms, even under heavy CPU and I/O stress.

B. Dynamic Parameter Identification

For the purpose of dynamic parameter identification, each joint was controlled in "velocity mode". Sinusoidal as well as polynomial velocity profiles were sent to the joints, in order to form exciting trajectories for the identification of the base parameters [8]. The friction and stiffness terms were computed in advance and therefore known during the dynamic parameter identification. Computed values of the PA-10 base parameters are listed in Appendix. The values π_2, π_{10} and π_{18} corresponding to first moment of inertia can be compared to values calculated by manufacturer's provided data [12]. The accuracy of the estimated values with respect to the real ones, is 99.3, 98.2 and 97% respectively.
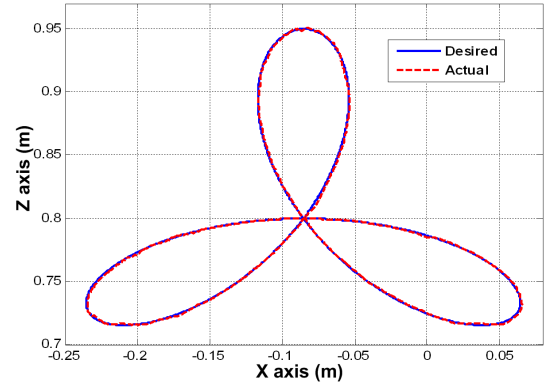
C. Experimental Verification of the Full Identified Model

The verification of the full model identified is performed through an end-effector trajectory tracking experiment. The trajectory of the end-effector was restricted to the xz plane of the base reference frame, while the orientation was kept constant. The trajectory is given by

$$
\begin{aligned}
x &= 0.085 \left(\cos(t) + \sin(2t) - 1 \right) \\
z &= -0.075 \left(\sin(t) + \cos(2t) - 1 \right) + 0.7248 \\
y &= 0.7
\end{aligned}
\tag{20}
$$

where t denotes time. This trajectory results to joint motions that are of different form of those used during identification experiments, thus providing an excellent mean of verification of the identified model. The control law implemented was chosen to have the simplest form in order to verify the identified model. An inverse dynamic controller was selected, given by

$$
\begin{aligned}
\mathbf{u} = \mathbf{B} \left(\ddot{\mathbf{q}}_d + \mathbf{K_V} \left(\dot{\mathbf{q}}_d - \dot{\mathbf{q}} \right) + \mathbf{K_P} \left(\mathbf{q}_d - \mathbf{q} \right) \right) + \\
\mathbf{C} \left(q, \dot{q} \right) + \mathbf{G} \left(q \right) + \mathbf{F} + \mathbf{S}
\end{aligned}
\tag{21}
$$

where $\mathbf{B}$, $\mathbf{C}$, matrices of the dynamic model equation defined in (17), $\mathbf{G}$, $\mathbf{F}$, $\mathbf{S}$ the gravity, friction and stiffness vector respectively, $\mathbf{K_V}$, $\mathbf{K_P}$ 7×7 diagonal positive definite matrices of gains and $\mathbf{q_d}$ the desired joint trajectories computed from the desired end-effector trajectory given in (20), using an inverse kinematics algorithm. The algorithm used is the Jacobian pseudo-inverse algorithm for redundant manipulators described in [11], with an added term to avoid joint limits. In Fig. 7 the trajectory followed by the end-effector is shown along with the desired, as well as the error in end-effector position in Cartesian space. As it can be seen, the end-effector moved along the desired trajectory with high accuracy. The maximum error in joint space was 0.15 deg, while the mean position error in Cartesian space was limited to 0.8 mm while the smaller value found in literature for the same experiment was at 2 cm in [1]. In Fig. 8 the torque sent to each joint during the trajectory tracking experiment is plotted. As it can been seen the feedback torque is very low with respect to the total torque $\mathbf{u}$ given in (21), which proves the high accuracy of the identified full model of the PA-10 robot arm.
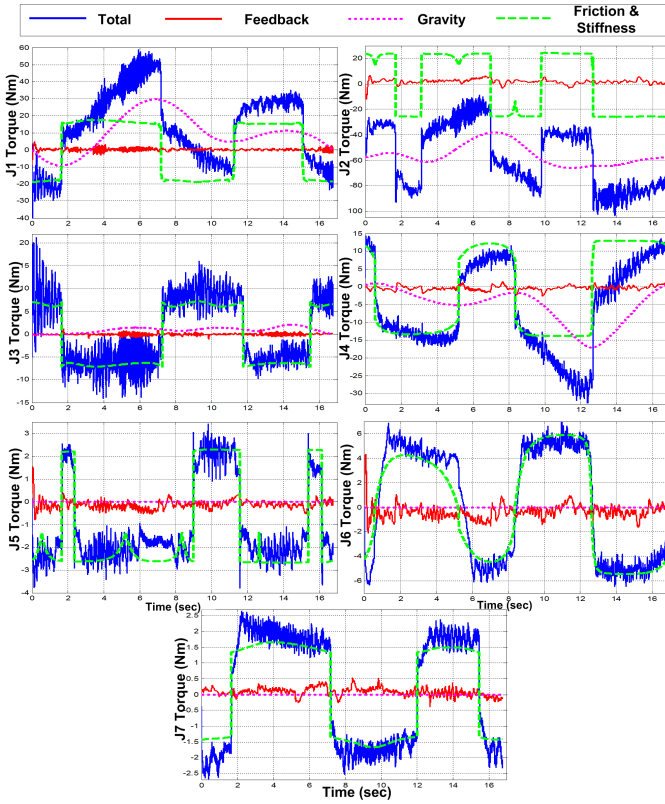
Fig. 8. Joints Torques during tracking experiment.

IV. CONCLUSION

In this paper the modeling and full identification and control of the Mitshibishi PA-10 robot arm was developed. A new non-linear friction model for the robot joints was constructed and experimentally identified, while the stiffness effect of the joints was also identified through experimental procedure in loaded conditions. The parameters of the dynamic model were grouped to an identifiable form, and identified through experiments. A model-based inverse dynamic controller was finally used to evaluate the identified model within a trajectory tracking experiment. In this experiment, the low feedback torque measured at the robot joints proved the model's accuracy. Consequently, as the Mitsubishi PA-10 robot arm is widely used in research laboratories world wide, the full model identified here is of high importance as it allows the implementation of any model-based controller, incorporating accurate models for friction and stiffness effects at the robot joints.

ACKNOWLEDGMENTS

APPENDIX

Base Parameters of the PA-10 robot arm

The base parameters of the PA-10 robot arm and their identified values are given by:

$$\pi_1 = \hat{I}_{1zzR} = \hat{I}_{1zz} + \hat{I}_{2yy} + k_r^2 I_{m_1} = 6.3376 \; Kgm^2$$
$$\pi_2 = M_{2yR} = \ell_{C_2y}m_2 - \ell_{C_3z}m_3 -$$
$$d_3\,(m_3 + m_4 + m_5 + m_6) = -7.3424 \; Kgm$$
$$\pi_3 = \hat{I}_{2xxR} = \hat{I}_{2xx} + \hat{I}_{3yy} + 2d_3\ell_{C_3z}m_3 +$$
$$d_3^2\,(m_3 + m_4 + m_5 + m_6) - \hat{I}_{2yy} = 2.9419 \; Kgm^2$$
$$\pi_4 = \hat{I}_{2yzR} = \hat{I}_{2yz} = 3.7152 \; Kgm^2$$
$$\pi_5 = \hat{I}_{2zzR} = \hat{I}_{2zz} + \hat{I}_{3yy} + 2d_3\ell_{C_3z}m_3 +$$
$$d_3^2\,(m_3 + m_4 + m_5 + m_6) + k_r^2 I_{m_2} = 4.2823 \; Kgm^2$$
$$\pi_6 = I_{m_3} = 4.7890 \cdot 10^{-4} \; Kgm^2$$
$$\pi_7 = \hat{I}_{3xxR} = \hat{I}_{3xx} + \hat{I}_{4yy} - \hat{I}_{3yy} = -1.5248 \; Kgm^2$$
$$\pi_8 = \hat{I}_{3zzR} = \hat{I}_{3zz} + \hat{I}_{4yy} = 3.8092 \; Kgm^2$$
$$\pi_9 = I_{m_4} = 2.0595 \cdot 10^{-4} \; Kgm^2$$
$$\pi_{10} = M_{4yR} = \ell_{C_4y}m_4 - \ell_{C_5z}m_5 -$$
$$d_5\,(m_5 + m_6) = -3.2317 \; Kgm$$
$$\pi_{11} = \hat{I}_{4xxR} = \hat{I}_{4xx} + \hat{I}_{5yy} + 2d_5\ell_{C_5z}m_5 +$$
$$d_5^2\,(m_5 + m_6) - \hat{I}_{4yy} = 0.7116 \; Kgm^2$$
$$\pi_{12} = \hat{I}_{4yzR} = \hat{I}_{4yz} = 0.4189 \; Kgm^2$$
$$\pi_{13} = \hat{I}_{4zzR} = \hat{I}_{4zz} + \hat{I}_{5yy} + 2d_5\ell_{C_5z}m_5 +$$
$$d_5^2\,(m_5 + m_6) = 0.4961 \; Kgm^2$$
$$\pi_{14} = I_{m_5} = 3.2303 \cdot 10^{-4} \; Kgm^2$$
$$\pi_{15} = \hat{I}_{5xxR} = \hat{I}_{5xx} + \hat{I}_{6yy} - \hat{I}_{5yy} = 0.2917 \; Kgm^2$$
$$\pi_{16} = \hat{I}_{5zzR} = \hat{I}_{5zz} + \hat{I}_{6yy} = 0.1309 \; Kgm^2$$
$$\pi_{17} = I_{m_6} = 2.5371 \cdot 10^{-4} \; Kgm^2$$
$$\pi_{18} = M_{6yR} = \ell_{C_6y}m_6 = 0.05377 \; Kgm$$
$$\pi_{19} = \hat{I}_{6xxR} = \hat{I}_{6xx} - \hat{I}_{6yy} = 0.1861 \; Kgm^2$$
$$\pi_{20} = \hat{I}_{6zzR} = \hat{I}_{6zz} = 0.0747 \; Kgm^2$$
$$\pi_{21} = I_{m_7} = 9.2458 \cdot 10^{-6} \; Kgm^2$$

REFERENCES

[1] C.W. Kennedy, and J.P. Desai, "Modeling and control of the Mitsubishi PA-10 robot arm harmonic drive system," IEEE Trans. Mechatronics, vol 10, no. 3, pp. 263-274, June 2005.

[2] T.D. Tuttle, "Understanding and modeling the behavior of a harmonic drive gear transmission," Masters Thesis, MIT Artificial Intelligence Laboratory, 1992.

[3] N. Kircanski, and A.A. Goldenberg, "An experimental study of nonlinear stiffness, hysteresis, and friction effects in robot joints with harmonic drives and torque sensors," Int. Jour. Robotics Research, vol 16, no. 2., pp. 214-239, 1997.

[4] H.D. Taghirad, and P.R. Belanger, "An experimental study on modelling and identification of harmonic drive systems," in the Proc. of the 35th Conf. on Decision and Control, vol. 4, pp. 4725 - 4730, 1996.

[5] B. Armstrong-Helouvry, *Control of machines with friction*, Kluwer Academic Publishers, 1991.

[6] Craig T. Johnson, and Robert D. Lorenz, "Experimental Identification of Friction and its Compensation in Precise, Position Controlled Mechanisms," IEEE Trans. Industry Applications, vol. 28, no. 6, November/December 1992.

[7] H. Olsson, K. J. Astrom, C. Canudas de Wit, M. Gafvert, and P. Lischinsky, "Friction models and friction compensation," European Journal of Control, vol. 4, no. 3, pp. 176195, 1998.

[8] K. Kozlowski, *Modeling and Identification in Robotics*, New York: Springer-Verlag, 1998.

[9] M.M. Olsen, and H.G. Peterson, "A New Method for Estimating Parameters of a Dynamic Robot Model," IEEE Trans. Robotics and Automation, vol. 17, no. 1, pp. 95-100, 2001.

[10] J.J. Craig, *Introduction to robotics: mechanics and control*, Addison Wesley, MA, 1989.

[11] L. Sciavicco, and B. Siciliano, *Modeling and Control of Robot Manipulators*, McGraw-Hill, New York, 1996.

[12] http://www.mhi.co.jp/kobe/mhikobe/products/mechatronic/download /new/loadfile/7axis.jpg

[13] W. Khalil, and E. Domhre, *Modeling, identification and control of robots*, Hermes Penton, London-Paris, 2002.